Journal of Organometallic Chemistry 948 (2021) 121912

Contents lists available at ScienceDirect

Journal of Organometallic Chemistry

journal homepage: www.elsevier.com/locate/jorganchem

Guanine base stabilized on the magnetic nanoparticles as recyclable catalyst “on water” for the synthesis of spirooxindole derivatives

Dariush Saberi*, Mohammad Bashkar, Arash Rezaei, Zohre Azizi, Khodabakhsh Niknam*

Department of Chemistry, Faculty of Nano and Bio Science and Technology, Persian Gulf University, Bushehr 75169 Iran

ARTICLE INFO

Article history:
Received 15 April 2021
Revised 7 May 2021
Accepted 26 May 2021
Available online 31 May 2021

Keywords:
Guanine
Bis-spirooxindoles
Heterogeneous base catalyst
Magnetic nanoparticles
“On water”

ABSTRACT

Guanine stabilized on the surface of silica-modified magnetic nanoparticles, by the propyl group as a linker, (Fe_3O_4@SiO_2-n-(propyl)-guanine), was prepared, identified and used as a recyclable base in the synthesis of novel spirooxindole compounds and highly substituted dihydro-2-oxopyrroles in aqueous media. Fe_3O_4@SiO_2-n-(propyl)-guanine was characterized via some spectroscopic and microscopic techniques such as Infrared spectroscopy (IR), X-ray diffraction spectroscopy (XRD), Energy dispersive X-ray spectroscopy (EDX), Vibrating sample magnetometry (VSM), Scanning electron microscopy (SEM), High resolution transmission electron microscopy (HR-TEM), Thermo-gravimetric analysis (TGA) and NMR-detected hydrogen/deuterium (H/D) exchange technique. The synthesized nanocomposite was employed as a new base catalyst for the synthesis of some novel spirooxindole compounds and highly substituted dihydro-2-oxopyrroles in aqueous media with good to excellent yields. This heterogeneous base catalyst could be recycled and reused up to ten times without appreciable loss of activity.

1. Introduction

The development of economical and environmentally friendly methods for the synthesis of organic compounds has received considerable attention in recent years. Base-catalyzed condensation and addition reactions are important in the industrial production of drugs, fragrances, and chemical intermediates [1–6]. The potential use of microporous and mesoporous base catalysts in fine chemical production is enormous [6,7]. In addition, the applications of amine-based silica mesopores were reported in adsorption, separation, and chromatography [8]. Moreover, solid base catalysts are used not only for condensation reactions but also in particular for asymmetric organic syntheses [9,10], other organic syntheses [11–18], solid-phase extraction and preconcentration of some metal ions [19], and catalytic hydrothermal liquefaction of macroalgae [20]. So, incorporating base functionality into microporous and mesoporous silicas also avoids the complex neutralization and separation steps needed to recover the homogeneous base catalysts from the reaction mixture. These silicas are particular interest in organic synthesis, green chemistry and industry because of their high selectivity, high yields, and the environmentally advantageous heterogeneity and reusability.

In addition, replacement or removal of hazardous solvents with green ones has been one of the targets of researchers in green synthesis. Water, as a green reaction medium, has attracted significant attention in view of extensive hydrogen bonding, cohesive energy density, high heat capacity, and large dielectric constant. In addition, the unique properties of water and its non-toxic nature, cost-effectiveness and non-inflammability raised its applicability [21-25].

Spirooxindole derivatives are an important class of heterocyclic compounds that exist in many natural compounds and alkaloids such as spirotryprostatins [26], horsfiline [27], pteropodine [28], alstonisine,[29] and gelsemine [30]. These compounds show a broad spectrum of pharmacological and biological activity such as antitumor [31], antifungal [32], antimicrobial [33], antimalarial [34], antitubercular [35], and anti-HIV properties [36]. Given the importance of such biological activities, green synthetic methods to prepare of these compounds have drawn more and more attention of chemists. To date, various methods for the preparation of spirooxindole scaffold has been widely developed under a variety of catalysts such as NH_4Cl [37], L-proline [38], p-TSA [39], amino-functionalized SBA-15 type mesoporous silica [40], Nano Ag/kaolin [41], Et_3N [42], DBU [43], nanocrystalline MgO [44], silica-bonded N-propyltriethylenetetramine (SBNPTT) [14], gluconic acid [45], tetrabutylammonium fluoride (TBAF) [46], lipase [47], $CaCl_2$ under sonication [48], NaCl under sonication [49], triethylbenzylammonium chloride (TEBA) [50], sulfonic acid functionalized SBA-15 [51], sulfated choline based heteropolyanion [52], $MnFe_2O_4$ nanoparti-

* Corresponding authors.
E-mail addresses: saberi_d@pgu.ac.ir (D. Saberi), niknam@pgu.ac.ir (K. Niknam).

https://doi.org/10.1016/j.jorganchem.2021.121912
0022-328X/

cles [53], piperidine under ultrasonic irradiation [54], ethylenediammonium diformate (EDDF) [55], Fe(III)-montmorillonite under ultrasonic irradiation [56], silica-bonded ionic liquids [57], SiO_2@g-C_3N_4 [58], caffeinium hydrogen sulfate [59], double salt of aluminum sulfate-sulfuric acid ($Al_4(SO_4)_5.(HSO_4)_2.24H_2O$) [60], cuprene [61], Fe_3O_4-np [62], $FeNi_3$–SiO_2 magnetic nanoparticles [63], Fe_3O_4@SiO_2-imid-PMA^n magnetic porous nanospheres, [64] and Fe_3O_4/COS@β-CD-SO_3H NPs [65]. However, most of these procedures have several limitations in terms of long reaction time, metal catalyst, environmentally hazardous, expensive reagents, harsh reaction conditions, and use of homogeneous catalyst. In addition, some of them suffer from procedure complexity and generation of mixtures of unsaturated nitriles and pyrans.

In continuous of our research on the preparation and development of amine-based silica as a stabilizing palladium nano particles [66–69], and also as green catalyst for the synthesis of many organic products, [11–14,70–74] herein we report the Fe_3O_4-silica-n-(propyl)-guanine as a new, eco-friendly, and solid base catalyst for the synthesis of some mono- and novel bis-spirooxindoles and highly substituted dihydro-2-oxopyrrole compounds in aqueous media.

2. Experimental section

2.1. General

All the reagents were purchased from Merck and Aldrich Chemical Companies. The reaction monitoring was accomplished by TLC on silica gel PolyGram SILG/UV254 plates. Melting points determined in open capillary tubes in a Barnstead Electrothermal 9100 BZ circulating oil melting point apparatus. The compounds were visualized by ^{1}H-NMR (400 MHz) and ^{13}C-NMR (100 MHz), and spectra were on recorded Bruker Avance instrument in DMSO-d_6 solvent with tetramethylsilane (TMS) as internal standard. FT-IR spectroscopy (Shimadzu FT-IR 8300 spectrophotometer) was employed for the characterization of the products. Mass spectra were recorded on a FINNIGAN-MAT 8430 mass spectrometer operating at 70 eV. X-ray diffraction (XRD) data were carried out using a Bruker D8 Advance Theta-2theta diffractometer. Magnetic properties of catalyst were obtained by vibrating sample magnetometer/Alternating Gradient Force Magnetometer (VSM/AGFM, MDK Co, Iran, www.mdk-magnetic.com). TGA was performed on a thermal analyzer with a heating rate of 20 °C min^{-1} over a temperature range of 30–600 °C under flowing compressed N_2. SEM images were observed using Philips XL 30 and S-4160 instruments. HR-TEM measurements were carried out at 200 kV (JEOL, JEM-2100F). Energy dispersive X-ray (EDX) spectroscopy (SiriusSD, England) was used for catalyst analysis.

2.1. Catalyst preparation

2.2.1. Preparation of silica-functionalized magnetite nanoparticles (Fe_3O_4@SiO_2)

Silica-coated magnetite nanoparticles were synthesized by a chemical co-precipitation technique of ferric and ferrous ions in alkali solution [9]. $FeCl_3.6H_2O$ (5 mmol) and $FeCl_2.4H_2O$ (2.5 mmol) salts were dissolved in 100 ml of deionized water under vigorous stirring (800 rpm). Then NH_4OH solution (25% w/w, 30 ml) was added to the mixture at room temperature. The addition of NH_4OH solution followed to maintain the reaction pH between 11 and 12 at which a black suspension was formed. The resulting black dispersion was continuously stirred for 1 hour at room temperature and then refluxed for another 1 hour. Coating of a layer of silica on the surface of the Fe_3O_4 nanoparticles was achieved by adding ethanol (40 mL) to the purified nanoparticles and heating for 1 hour at 40 °C. Subsequently, tetraethyl orthosilicate (TEOS; 10 mL) was charged to the reaction vessel, the mixture was continuously stirred for 24 hours. The silica coated nanoparticles (Fe_3O_4@SiO_2) were collected using a magnet, followed by washing five times with EtOH and diethyl ether, respectively, and drying at 100 °C in vacuum for 12 hours.

2.2.2. Modification of Fe_3O_4@SiO_2 with propyl chloride (Fe_3O_4@SiO_2-n-(propyl)-Cl)

Fe_3O_4@SiO_2 (1 g), prepared in the previous step, was dispersed in toluene (50 mL) by an ultrasound bath for 15 minutes. Then, to the mixture was added 3-Chloropropyl triethoxysilane (2 mL) drop-wise, and it was refluxed at 110°C for 24 hours. Nanoparticles were obtained through separation by a magnet, washed several times with toluene, water and ethanol, respectively and drying in an oven at 80 °C for 8 h.

2.2.3. Synthesis of magnetite nanoparticles silica-functionalized-guanine (Fe_3O_4@SiO_2–n-(propyl)-guanine)

Preceding synthesized Fe_3O_4@SiO_2-n-(propyl)-Cl nanoparticles (1 g) was added to a 100 mL balloon containing anhydrous dimethyl sulfoxide (50 mL) and subjected to ultrasound for 15 minutes. Guanine (4 mmol) and triethylamine (5 mmol) were then added to the mixture and refluxed for 48 h. The precipitate formed was separated by a strong magnet and washed with water (3 × 30 mL) and finally dried in a vacuum oven.

2.3. General procedure for the synthesis of spirooxindoles ***4a-t***

A mixture of isatin derivatives (1 mmol), 1,3-dicarbonyl compound (1 mmol), reactive methylene compound (1 mmol) and Fe_3O_4@SiO_2-n-(propyl)-guanine (0.02 g) in water (5 mL) was stirred at 70°C and progress of the reaction was monitored by TLC. After completion of the reaction, the mixture was cooled to room temperature and the catalyst easily separated from the reaction mixture by using an external magnet and washed twice with distilled water (2 × 5 mL), ethanol (2 × 5 mL), and acetone (2 × 5 mL) respectively. The precipitate formed in the reaction vessel was filtered and dried, washing with distilled water at room temperature. To obtain a pure product, the dried precipitate was recrystallized using of ethanol 96%. All the products were known and characterized by comparing their spectral (IR, ^{1}H- and ^{13}C-NMR), TLC, and physical data with those reported in the literature. Spectral information for some compounds is given below:

2-amino-2′,5-dioxo-5,6,7,8-tetrahydrospiro[chromene-4,3′-indoline]-3-carbonitrile (Table 2, **4a)**: White powder, m.p. 305–308°C (Lit. [75]; 307–310°C). ^{1}H-NMR (400 MHz, DMSO-d6) δ (ppm): 1.88–1.99 (m, 2H), 2.22–2.27 (m, 2H), 2.66–2.69 (m, 2H), 6.79 (d, J = 8.0 Hz,1H), 6.90 (t, J = 8.0 Hz, 1H), 7.02 (d, J = 8.0 Hz,1H), 7.15 (d, J = 8.0 Hz,1H), 7.25 (s, 2H, NH2), 10.42 (s, 1H, NH). ^{13}C-NMR (100 MHz, DMSO-d6) δ (ppm): 20.3, 27.2, 36.8, 47.3, 57.9, 109.6, 112.3, 117.9, 122.1, 123.7, 128.6, 135.0, 142.5, 159.1, 166.5, 178.6, 195.5.

2-amino-5′-methoxy-2′,5-dioxo-5,6,7,8-tetrahydrospiro[chromene-4,3′-indoline]-3-carbonitrile (Table 2, **4b)**: White powder, m.p. 273–275°C. (Lit. [60]; 272–275°C). ^{1}H-NMR (400 MHz, DMSO-d6) δ (ppm): 1.91–1.98 (m, 2H), 2.23–2.27 (m, 2H), 2.65–2.68 (m, 2H), 3.69 (s, 3H), 6.65 (d, J = 2.1 Hz, 1H), 6.71–6.72 (m, 2H), 7.23 (s, 2H, NH_2), 10.23 (s, 1H, NH). ^{13}C-NMR (100 MHz, DMSO-d6) δ (ppm): 20.2, 27.2, 36.9, 47.8, 55.8, 58.1, 109.9, 110.8, 112.3, 113.0, 117.9,135.8, 136.3, 155.4, 159.1, 166.5, 178.5, 195.5.

2-amino-5′-methyl-2′,5-dioxo-5,6,7,8-tetrahydrospiro[chromene-4,3′-indoline]-3-carbonitrile (Table 2, **4c)**: White powder, m.p. 274–276°C. (Lit. [76]; 275–277°C). ^{1}H-NMR (400 MHz, DMSO-d6) δ (ppm): 1.92–1.97 (m, 2H), 2.22–2.29 (m, 5H), 2.66–2.69 (m, 2H), 6.65 (d, J = 8.0 Hz, 1H), 6.83 (s, 1H),

6.95 (d, J = 8.0 Hz, 1H), 7.22 (s, 2H, NH_2), 10.31 (s, 1H, NH). ^{13}C-NMR (100 MHz, DMSO-d6) δ (ppm): 20.3, 21.2, 27.2, 36.9, 47.4, 58.2, 109.4, 112.4, 117.9, 124.3, 128.9, 130.9, 135.1, 140.0, 159.1, 166.4, 178.6, 195.5.

2-amino-5′-nitro-2′,5-dioxo-5,6,7,8-tetrahydrospiro[chromene-4,3′-indoline]-3-carbonitrile (Table 2, **4g**): Bright yellow powder, m.p. 306–308°C. (Lit. [77]; 306–307°C). ^{1}H-NMR (400 MHz, DMSO-d6) δ (ppm): 1.90–2.05 (m, 2H), 2.26–2.29 (m, 2H), 2.69–2.72 (m, 2H), 7.03 (d, J = 8.0 Hz, 1H), 7.47 (s, 2H, NH_2), 8.05 (s, 1H), 8.17 (d, J = 8.0 Hz, 1H), 11.20 (s,1H, NH). ^{13}C-NMR (100 MHz, DMSO-d6) δ (ppm): 20.1, 27.3, 36.6, 47.5, 56.4, 109.8, 111.3, 117.6, 119.7, 126.2, 136.0, 142.9, 149.0, 159.4, 167.7, 179.2, 196.0.

2-amino-7,7-dimethyl-2′,5-dioxo-5,6,7,8-tetrahydrospiro[chromene-4,3′-indoline]-3-carbonitrile (Table 2, **4h**): White powder, m.p. 290–292°C. (Lit. [78]; 290-292°C). ^{1}H NMR (400 MHz, DMSO-d6) δ (ppm): 1.00 (s, 3H), 1.04 (s, 3H), 2.10 (d, J = 12.8 Hz, 1H), 2.18 (d, J = 12.8 Hz, 1H), 2.54 (d, J = 14.1 Hz, 1H), 2.59 (d, J = 14.1 Hz, 1H), 6.79 (d, J = 6.0 Hz, 1H), 6.89 (dt, J_1 = 6.0 Hz, J_2 = 0.8 Hz, 1H), 6.98 (d, J = 5.8 Hz, 1H), 7.14 (dt, J_1 = 6.2 Hz, J_2 = 0.8 Hz, 1H), 7.24 (s, 2H, NH_2), 10.41 (s, 1H, NH). ^{13}C-NMR (100 MHz, DMSO-d6) δ (ppm): 26.9, 27.5, 31.9, 46.7, 49.9, 57.4, 109.2, 110.7, 117.3, 121.6, 122.9, 128.1, 134.3, 142.0, 158.7, 146.1, 177.9, 194.8.

2-amino-5′-methoxy-7,7-dimethyl-2′,5-dioxo-5,6,7,8-tetrahydrospiro[chromene-4,3′-indoline]-3-carbonitrile (Table 2, **4i**): White powder, m.p. 270–272°C. (Lit. [60]; 270–272°C). ^{1}H-NMR (400 MHz, DMSO-d6) δ (ppm): 1.01 (s, 3H), 1.03 (s, 3H), 2.08–2.18 (m, 2H), 2.55 (m, 2H), 3.65 (s,3H), 6.60 (s, 1H), 6.68–6.70 (m, 2H),7.23 (s, 2H, NH_2), 10.22 (s, 1H, NH). ^{13}C-NMR (100 MHz, DMSOd6) δ (ppm): 27.6, 28.0, 32.4, 47.7, 50.5, 55.8, 58.1, 110.0, 110.6, 111.2, 113.0, 117.9, 135.9, 136.2, 155.4, 159.2, 164.6, 178.4, 195.4.

2-amino-5′,7,7-trimethyl-2′,5-dioxo-5,6,7,8-tetrahydrospiro[chromene-4,3′-indoline]-3-carbonitrile (Table 2, **4j**): White powder, m.p. 276–279°C. (Lit. [78]; 279–280°C). ^{1}H-NMR (400 MHz, DMSO-d6) δ (ppm): 1.01 (s, 3H), 1.03 (s, 3H), 2.09–2.14 (m, 2H), 2.20 (s, 3H), 2.55 (m, 2H), 6.67 (d, J = 8.0 Hz, 1H), 6.78 (s, 1H), 6.93–6.94 (m, 1H), 7.21 (s, 2H, NH_2), 10.29 (s, 1H, NH). ^{13}C-NMR (100 MHz, DMSO-d6) δ (ppm): 21.2, 27.7, 27.9, 32.4, 47.3, 50.5, 58.1, 109.5, 111.3, 117.9, 124.1, 128.9, 130.9, 135.0, 140.1, 159.2, 164.5, 178.5, 195.4.

2-amino-7,7-dimethyl-5′-nitro-2′,5-dioxo-5,6,7,8-tetrahydrospiro[chromene-4,3′-indoline]-3-carbonitrile (Table 2, **4n**): White powder, m.p. 302–305°C. (Lit. [79]; 302–304°C). ^{1}H-NMR (400 MHz, DMSO-d6) δ (ppm): 1.05 (s, 6H), 2.14–2.24 (m, 2H), 2.57–2.71 (m, 2H), 7.05 (d, J = 8.0 Hz. 1H), 7.49 (s, 2H, NH_2), 7.98–7.99 (m, 1H), 8.17 (d, J = 8.0 Hz, 1H), 11.20 (s, 1H, NH). ^{13}C-NMR (100 MHz, DMSO-d6) δ (ppm): 27.5, 28.2, 32.5, 47.4, 50.3, 56.3, 109.9, 110.2, 117.6, 119.4, 126.3, 135.8, 142.9, 149.1, 159.6, 165.7, 179.1, 195.9.

*2.4. General procedure for the synthesis of bis-spirooxindoles **6a-i***

Initially, bis(isatin) derivatives (**5**) have been synthesized according to the previously reported procedure [80]. Briefly, NaH (55 mmol, 1.32 g) was added to a solution of isatin derivatives (50 mmol) in DMF 25 mL at 0 °C and resulting mixture was stirred at that temperature for 0.5 h and then was warmed to room temperature. After this time, O-bis(bromomethyl)benzene (25 mmol, 6.60 g) was added and resulting solution was stirred at 80 °C for 8h. After completion, the reaction mixture was cooled to room temperature and excess amounts of water (250 mL) was added and resulting precipitates was filtered and dried. Crude products were recrystallized from hot ethanol to obtain the pure ones. Bis(isatin) compound (1 mmol) was added to a flask containing a mixture of malononitrile (1mmol), 1,3-dicarbonyl compound (1 mmol) and Fe_3O_4@SiO_2-n-(propyl)-guanine (0.02 g) in water (3 mL) and the mixture stirred at 80°C. After completion, the reaction mixture was cooled to room temperature, the catalyst easily separated from the reaction mixture by using an external magnet and washed twice with distilled water (2 × 5 mL), ethanol (2 × 5 mL), and acetone (2 × 5 mL) respectively. The crude product, formed in the reaction vessel, was filtered and purified by recrystallization from ethanol 96%. All the products (besides compounds **5f, 6h** and **6i**) were known and characterized by comparing their spectral (IR, ^{1}H- and ^{13}C-NMR, Mass), TLC, and physical data with those reported in the literature. The spectra of new compound (**5f, 6h** and **6i)** are given in the supporting information file. Spectral information for some compounds is given below:

1,1′-(1,2-Phenylenebis(methylene))bis(indoline-2,3-dione) (**5a**): Orange powder, m.p. 243-248°C. (Lit [60]. 243-248°C). ^{1}H-NMR (400 MHz, DMSO-d6): δ (ppm) 5.12 (s, 4H), 7.01 (d, 2H, J = 8.0 Hz, Ar), 7.16 (t, 2H, J = 8.0 Hz, Ar), 7.19–7.22 (m, 2H, Ar), 7.35–7.38 (m, 2H, Ar), 7.58–7.63 (m, 4H, Ar). ^{13}C-NMR (100 MHz, DMSO-d6): δ (ppm) 41.3, 111.8, 118.5, 123.9, 125.0, 126.9, 128.0, 133.1, 138.3, 150.9, 159.1, 183.4; MS (EI, 70 eV): m/z (%) = 397 (M^+ + 1, base peak).

1,1′-(1,2-Phenylenebis(methylene))bis(5-methylindoline-2,3-dione) (**5b**): Orange powder, m.p. 286-290°C. (Lit [60]. 286-290°C). ^{1}H-NMR (400 MHz, DMSO-d6): δ (ppm) 2.31 (s, 6H, 2 × CH_3), 5.12 (s, 4H), 6.92 (m, 2H, Ar), 7.20–7.24 (m, 2H, Ar), 7.33– 7.35 (m, 2H, Ar), 7.36–7.47 (m, 4H, Ar); MS (EI, 70 eV): m/z (%) = 425 (M^+, 50%), 304 (base peak).

1,1′-(1,2-Phenylenebis(methylene))bis(5-bromoindoline-2,3-dione) (**5c**): Orange powder, m.p. 273-276°C. (Lit [60]. 273-276°C). ^{1}H-NMR (400 MHz, DMSO-d6): δ (ppm) 5.13 (s, 4H), 6.98– 7.01 (m, 2H, Ar), 7.18–7.25 (m, 2H, Ar), 7.38–7.42 (m, 2H, Ar), 7.79–7.82 (m, 4H, Ar). ^{13}C-NMR (100 MHz, DMSO-d6): δ (ppm) 41.3, 113.9, 115.6, 120.4, 126.8, 127.1, 128.0, 132.8, 139.9, 149.8, 158.8, 182.1; MS (EI, 70 eV): m/z (%) = 554 (M^+ + 2, 5%), 552 (M^+,5%), 274 (base peak).

1,1′-(1,2-Phenylenebis(methylene))bis(5-chloroindoline-2,3-dione) (**5d**): Orange powder, m.p. 250 > °C. ^{1}H-NMR (400 MHz, DMSO-d_6): δ (ppm) 5.13 (s, 4H), 7.05 (d, 2H, J = 8.0 Hz, Ar), 7.19–7.25 (m, 2H, Ar), 7.38–7.42 (m, 2H, Ar), 7.66–7.70 (m, 4H, Ar). ^{13}C-NMR (100 MHz, DMSO-d_6): δ (ppm) 41.4, 113.5, 120.0, 124.4, 126.9, 128.0, 128.1, 132.9, 137.1, 149.4, 158.9, 182.3; MS (EI, 70 eV): m/z (%) = 465 (M^+ + 1, base peak).

1,1′-(1,2-Phenylenebis(methylene))bis(5-nitroindoline-2,3-dione) (**5e**): Orange powder, m.p. 215-220°C. (Lit [60]. 215-220°C). ^{1}H-NMR (400 MHz, DMSO-d6): δ (ppm) 5.26 (s, 4H), 7.20– 7.26 (m, 4H, Ar), 7.45–7.51 (m, 2H, Ar), 7.34–7.35 (m, 2H, Ar), 8.50–8.54 (m, 2H, Ar). ^{13}C-NMR (100 MHz, DMSO-d6): δ (ppm) 41.7, 112.2, 119.2, 119.5, 126.9, 128.0, 132.6, 133.1, 143.7, 155.2, 159.8, 181.2; MS (EI, 70 eV): m/z (%) = 487 (M^+ + 1, 6%), 485 (70%), 191 (base peak).

1,1′-(1,2-phenylenebis(methylene))bis(5-methoxyindoline-2,3-dione) **(5f)**: light red powder, m.p. 253-256°C. ^{1}H-NMR (400 MHz, DMSO-d6): δ (ppm) 3.79 (s, 6H, OMe), 5.10 (s, 4H, CH_2), 6.95 (d, J = 6.0 Hz, 2H, Ar), 7.18-7.26 (m, 6H, Ar), 7.33-7.38 (m, 2H, Ar). ^{13}C-NMR (100 MHz, DMSO-d6): δ (ppm) 41.2, 56.34, 109.7, 112.8, 118.9, 124.1, 127.0, 128.0, 133.2, 144.7, 156.31, 159.1, 183.7; MS (EI, 70 eV): m/z (%) = 457 (M^+ + 1, base peak).

1′,1′′′-(1,2-Phenylenebis(methylene))bis(2-amino-7,7-dimethyl-2′,5-dioxo-5,6,7,8 tetrahydrospiro[chromene-4,3′-indoline]-3-carbonitrile) (Table 3, **6a**): White powder, m.p. 303-304°C. (Lit [60]. 303-304°C). υ_{max} (KBr) 3150, 2195, 1737, 1680, 1609 cm^{-1}. ^{1}H-NMR (400 MHz, DMSO-d6): δ (ppm) 1.04 (s, 6H, 2 × CH_3), 1.05 (s, 6H, 2 × CH_3), 2.13–2.26 (m,4H), 2.58–2.68 (s, 4H), 5.10 (s, 4H), 6.84–6.87 (m, 2H, Ar), 6.99–7.04 (m, 2H, Ar), 7.09–7.22 (m, 6H, Ar), 7.35 (s, 4H, 2 × NH_2), 7.53–7.56 (m, 2H, Ar). ^{13}C-NMR (100 MHz, DMSO-d6): δ (ppm) 27.6, 28.1, 32.5, 41.5, 47.2, 50.4, 57.7, 109.7,

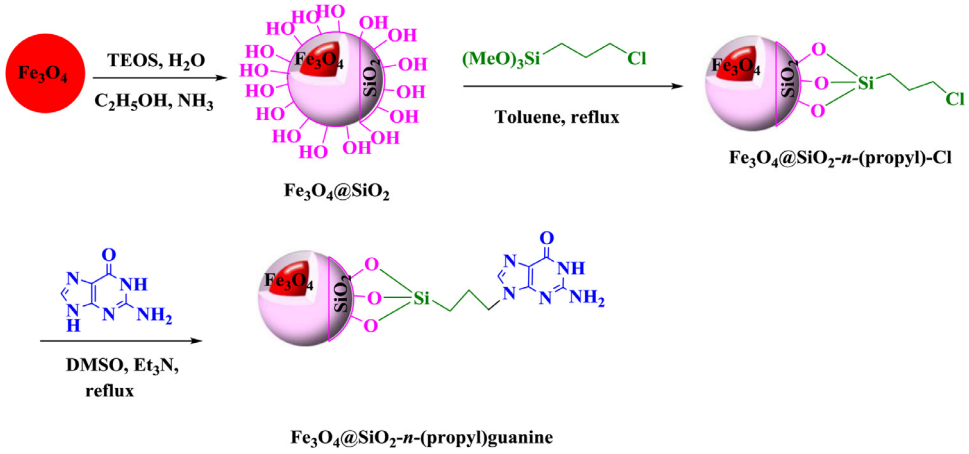

Scheme 1. Steps of stabilizing guanine on the surface of magnetic nanoparticles

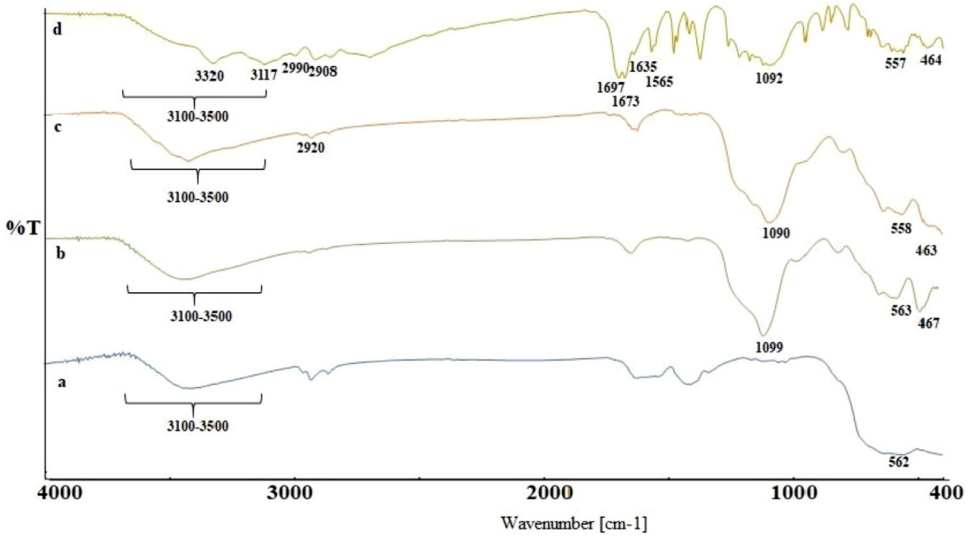

Fig. 1. FT-IR spectra of a) Fe_3O_4; b) Fe_3O_4@SiO_2; c) Fe_3O_4@SiO_2-n-(propyl)-Cl; d) Fe_3O_4@SiO_2-n-(propyl)-guanine

111.1, 118.0, 123.2, 123.4, 126.7, 127.4, 128.8, 133.6, 134.1, 143.4, 159.4, 166.1, 177.3, 196.6; MS (EI, 70 eV): m/z (%) = 773 (M^+ + 1, 10%), 274 (basepeak).

1′,1′′′-(1,2-phenylenebis(methylene))bis(2-amino-2′,5-dioxo-5,6,7,8-tetrahydrospiro[chromene-4,3′-indoline]-3-carbonitrile) (Table 3, **6b**): White powder, m.p. 297-300°C. (Lit [60]. 297-300°C). ^{1}H-NMR (400 MHz, DMSO-d6): δ (ppm) 1.94–2.02 (m, 4H), 2.28–2.33 (m, 4H), 2.71–2.75 (m, 4H), 5.11 (s, 4H), 6.85–6.88 (m, 2H, Ar), 7.03–7.05 (m, 2H, Ar), 7.12–7.22 (m, 6H, Ar), 7.36 (s, 4H, 2 × NH_2), 7.57–7.58 (m, 2H, Ar). ^{13}C-NMR (100 MHz, DMSO-d6): δ (ppm) 20.3, 27.3, 36.8, 41.5, 47.3, 57.8, 109.5, 112.2, 118.0, 123.1, 123.6, 126.7, 127.4, 128.8, 133.6, 134.3, 143.3, 159.3, 167.0, 177.4, 195.7; MS (EI, 70 eV): m/z (%) = 717 (M^+ + 1, 2%), 304 (base peak).

1,1′′-(1,2-phenylenebis(methylene))bis(7′-amino-2,2′,4′-trioxo-1′,2′,3′,4′-tetrahydrospiro[indoline-3,5′-pyrano[2,3-d]pyrimidine]-6′-carbonitrile) (Table 3, **6c)**: White powder, m.p. 194-202°C. (Lit [60]. 194-202°C). ^{1}H-NMR (400 MHz, DMSO-d6): δ (ppm) 5.14 (m, 4H), 6.85–6.89 (m, 2H, Ar), 7.03–7.10 (m, 4H, Ar), 7.22–7.27 (m, 2H, Ar), 7.32 (d, 2H, J = 8.0 Hz, Ar), 7.50 (s, 4H, 2 × NH_2), 11.26 (s, 2H, NH), 12.44 (s, 2H, NH). ^{13}C-NMR (100 MHz, DMSO-d6): δ (ppm) 41.5, 47.1, 58.1, 87.1, 109.7, 117.6, 123.2, 124.2, 126.4, 127.3, 129.1, 133.3, 133.4, 143.4, 149.7, 154.1, 158.9, 162.1, 177.0; MS (EI, 70 eV): m/z (%) = 749 (M^+ + 1, 5%), 274 (base peak).

1,1′′-(1,2-phenylenebis(methylene))bis(7′-amino-1′,3′-dimethyl-2,2′,4′-trioxo-1′,2′,3′,4′-tetrahydrospiro[indoline-3,5′-pyrano[2,3-d]pyrimidine]-6′-carbonitrile) (Table 3, **6d)**: White powder, m.p. 232-240°C. (Lit [60]. 232-240°C). υ_{max} (KBr) 3200, 2200, 1737, 1723, 1689, 1611 cm$^{-1.}$ ^{1}H-NMR (400 MHz, DMSO-d6): δ (ppm) 3.09 (s, 6H, 2 × CH_3), 3.44 (s, 6H, 2 × CH_3), 5.15 (m, 4H), 6.89–6.90 (m, 2H, Ar), 7.03–7.10 (m, 2H, Ar),7.14–7.32 (m, 6H, Ar), 7.72 (s, 4H, 2 × NH_2). ^{13}C-NMR (100 MHz, DMSO-d6): δ (ppm) 28.2, 29.9, 41.8, 47.8, 57.9, 87.4, 109.7, 117.6, 123.2, 124.2, 127.1, 127.5, 129.1, 133.4, 133.6, 143.5, 150.1, 152.7, 153.8, 160.1, 176.9; MS (EI, 70 eV): m/z (%) = 804 (M^+, 0.1%), 274 (base peak).

1′,1′′′-(1,2-phenylenebis(methylene))bis(2-amino-5′,7,7-trimethyl-2′,5-dioxo-5,6,7,8-tetrahydrospiro[chromene-4,3′-indoline]-3-carbonitrile) (Table 3, **6e)**: White powder, m.p. 204-209°C. (Lit [60]. 204-209°C). υ_{max} (KBr) 3200, 2192, 1738, 1667, 1601 cm^{-1}. ^{1}H-NMR (400 MHz, DMSO-d6): δ (ppm) 1.07 (s, 12H, 4 × CH_3), 2.19–2.31 (m, 10H, CH2, and CH_3), 2.64 (s, 4H), 5.08 (s, 4H), 6.75 (d, 2H, J = 8.0 Hz, Ar), 6.96–7.03 (m, 4H, Ar), 7.11–7.16 (m, 2H, Ar), 7.37 (s, 4H, 2 × NH_2), 7.53–7.57 (m, 2H, Ar). ^{13}C-NMR (100 MHz, DMSO-d6): δ (ppm)21.1, 27.8, 27.9, 32.5, 41.5, 47.3, 50.5, 57.9, 57.9,109.5, 111.2, 118.1, 124.1, 126.7, 127.3, 129.0, 132.1, 133.7, 134.2, 141.1, 159.4,165.0, 177.2, 195.6; MS (EI, 70 eV): m/z (%) = 801 (M^+ + 1, 10%), 304 (base peak).

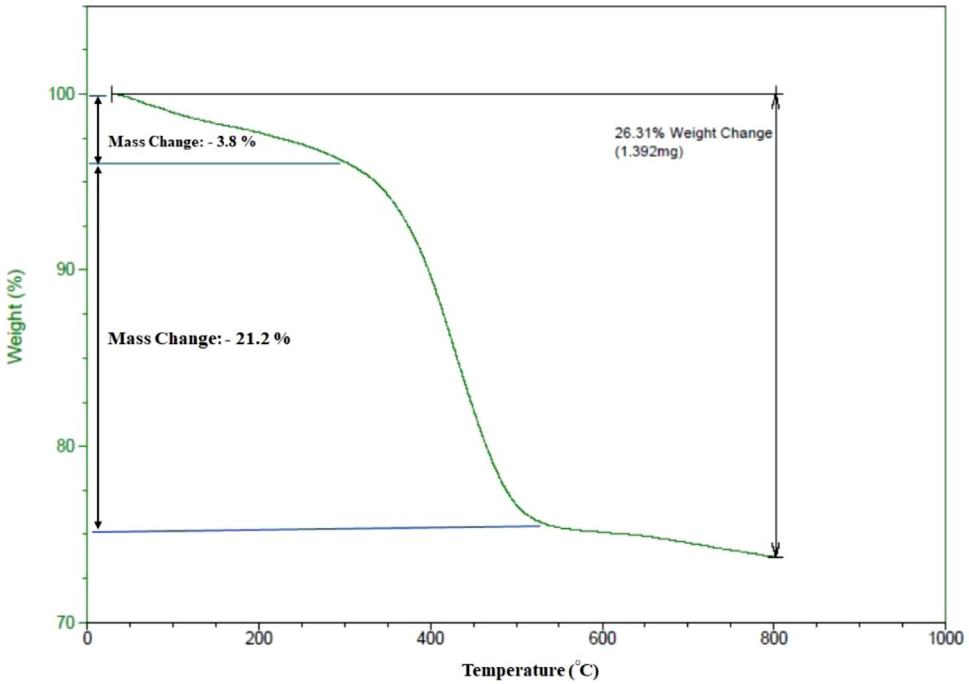

Fig. 2. Thermogravimetric weight loss plot for the Fe_3O_4@SiO_2-n-(propyl)-guanine

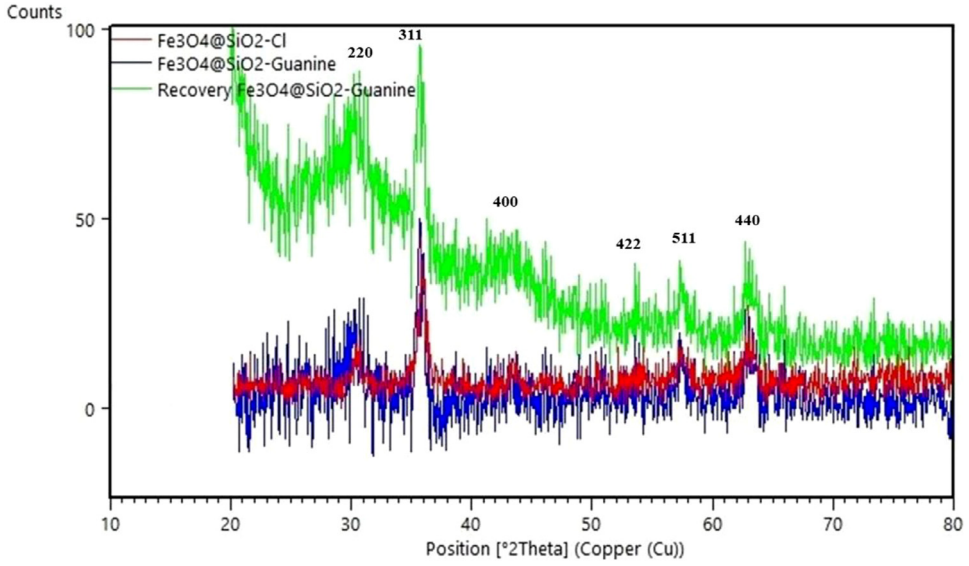

Fig. 3. XRD pattern of the Fe_3O_4@SiO_2–Cl, Fe_3O_4@SiO_2-n-(propyl)-guanine and the recovered Fe_3O_4@SiO_2-n-(propyl)-guanine after ten consecutive runs

1′,1′″-(1 phenylenebis(methylene))bis(2-amino-5′-bromo-7,7-dimethyl-2′,5-dioxo-5,6,7,8-tetrahydrospiro[chromene-4,3′-indoline]-3-carbonitrile,2-) (Table 3, **6f**): White powder, m.p. 311-315°C. (Lit [60]. 311-315°C). ^{1}H-NMR (400 MHz, DMSO-d6): δ (ppm) 1.06 (s, 6H, 2 × CH_3), 1.08 (s, 6H, 2 × CH_3), 2.18–2.30 (m, 4H), 2.56–2.71 (m, 4H), 5.13 (s, 4H), 6.83–6.86 (m, 2H, Ar), 7.13–7.16 (m, 2H, Ar), 7.41–7.54 (m, 10H, NH_2 and Ar). ^{13}C-NMR (100 MHz, DMSO-d6): δ (ppm) 27.6, 28.1, 32.5, 47.4, 50.4, 57.0, 110.5, 111.7, 115.0, 117.9, 126.4, 126.5, 127.5, 131.5, 133.3, 136.5, 142.7, 159.6, 165.6, 177.0, 195.8; MS (EI, 70 eV): m/z (%) = 274 (base peak).

1′,1′″-(1,2-phenylenebis(methylene))bis(2-amino-7,7-dimethyl-5′-nitro-2′,5-dioxo-5,6,7,8-tetrahydrospiro[chromene-4,3′-indoline]-3-carbonitrile) (Table 3, **6g**): White powder, m.p. 315-320°C. (Lit [60]. 315-320°C). ^{1}H-NMR (400 MHz, DMSO-d6): δ (ppm) 1.07 (s, 6H, 2 × CH_3), 1.09 (s, 6H, 2 × CH_3), 2.19–2.33 (m, 4H), 2.58–2.78 (m, 4H), 5.30 (s, 4H), 7.13–7.19 (m, 4H, Ar), 7.50–7.53 (m, 2H, Ar), 7.61 (s, 4H, Ar), 8.16–8.17 (s, 2H, NH_2), 8.23–8.27 (m, 2H, Ar). ^{13}C-NMR (100 MHz, DMSO-d6): δ (ppm) 27.5, 28.3, 32.6, 41.9, 47.3, 50.3, 56.2, 110.0, 110.1, 117.8, 119.3, 126.2, 126.3, 127.7, 132.9, 135.2, 143.7, 149.3, 159.8, 166.3, 178.0, 196.1; MS (EI, 70 eV): m/z (%) = 862 (M^+, 0.1%), 139 (base peak).

1,1′′-(1,2-phenylenebis(methylene))bis(7′-amino-1′,3′-dimethyl-2,2′,4′-trioxo-1′,1′″-(1,2-phenylenebis(methylene))bis(2-amino-5′-chloro-7,7-dimethyl-2′,5-dioxo-5,6,7,8-tetrahydrospiro[chromene-4,3′-indoline]-3-carbonitrile) (Table 3, **6h**): White powder, m.p. 325-328°C. υ_{max} (KBr) 3250,3290, 2192, 1735, 1670 cm^{-1}. ^{1}H-NMR (400 MHz, DMSO-d6): δ (ppm) 1.07 (s, 6H, CH_3), 1.08 (s, 6H, CH_3), 2.23–2.26 (m, 4H, CH_2), 2.56–2.71 (m, 4H, CH_2), 5.14 (s, 4H, CH_2), 6.88–6.91 (m, 2H, Ar), 7.12–7.18 (m, 2H, Ar), 7.28–7.31 (m, 4H, Ar),

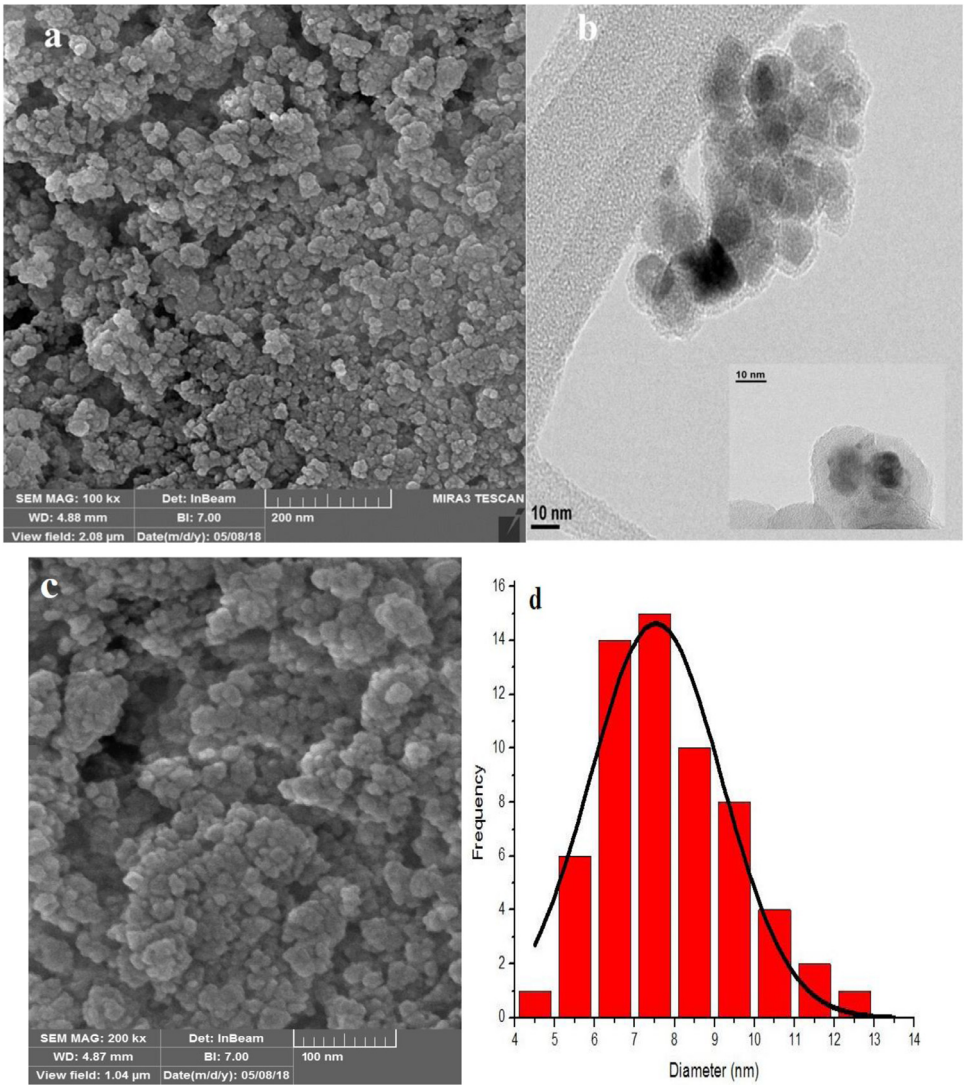

Fig. 4. SEM image (a), and HR-TEM micrograph (b), of the catalyst and SEM image (c) of the recovered catalyst after ten consecutive runs. The histogram of nanoparticles size by means of the TEM image (d) of the Fe_3O_4@SiO_2-n-(propyl)-guanine

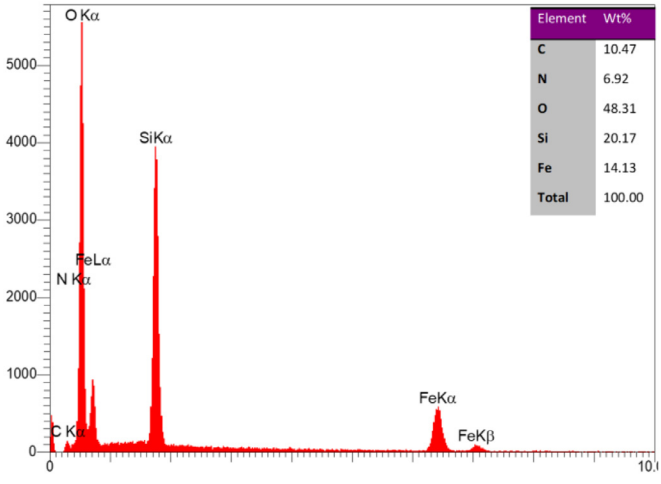

Fig. 5. EDX Pattern of the catalyst

7.48–7.54 (m, 6H, NH_2 and Ar). ^{13}C-NMR (100 MHz, DMSO-d6): δ (ppm) 27.7, 28.1, 32.5, 41.6, 47.4, 50.4, 57.0, 110.5, 111.2, 118.0, 123.8, 126.6, 127.3, 127.5, 128.7, 133.3, 136.1, 142.3, 159.6, 165.6, 177.1, 195.9; MS (EI, 70 eV): m/z (%) = 841 (base peak).

1′,1′″-(1,2-phenylenebis(methylene))bis(2-amino-5′-methoxy-7,7-dimethyl-2′,5 -dioxo-5,6,7,8-tetrahydrospiro[chromene-4,3′-indoline]-3-carbonitrile) (Table 3, **6i**): White powder, m.p. 200 <°C. υ_{max} (KBr) 3301, 1738, 1690, 1601 cm^{-1}. ^{1}H-NMR (400 MHz, DMSO-d6): δ (ppm) 1.05 (s, 6H, CH_3), 1.23 (s, 6H, CH_3), 2.08 – 2.27 (m, 4H, CH_2), 2.54–2.73 (m, 4H, CH_2), 3.68 (s, 6H, OMe), 5.04 (s, 4H, CH_2), 6.74 – 6.76 (m, 4H, Ar), 7.09–7.12 (m, 2H, Ar), 7.35 (s, 4H, NH_2), 7.50–7.54 (m, 2H, Ar), 7.68 – 7.72 (m, 2H, Ar). ^{13}C-NMR (100 MHz, DMSO-d6): δ (ppm) 27.6, 28.1, 32.7, 41.2, 47.7, 50.5, 55.7, 58.1, 110.0, 110.6, 111.2, 113.0, 117.9, 126.6, 127.6, 132.8, 135.2, 136.1, 155.5, 158.4, 164.9, 178.6, 195.4.

3. Results and discussion

As shown in Scheme 1, Fe_3O_4@SiO_2-n-(propyl)-guanine was prepared in several steps (for details see Experimental section). (Scheme 1).

Prepared catalyst was then characterized using various microscopic and spectroscopic techniques such as FT-IR, XRD, VSM, ICP, TGA, SEM, EDX, HRTEM and NMR. The FT-IR spectra of the prepared Fe_3O_4, Fe_3O_4@SiO_2, Fe_3O_4@SiO_2-n-(propyl)-Cl and

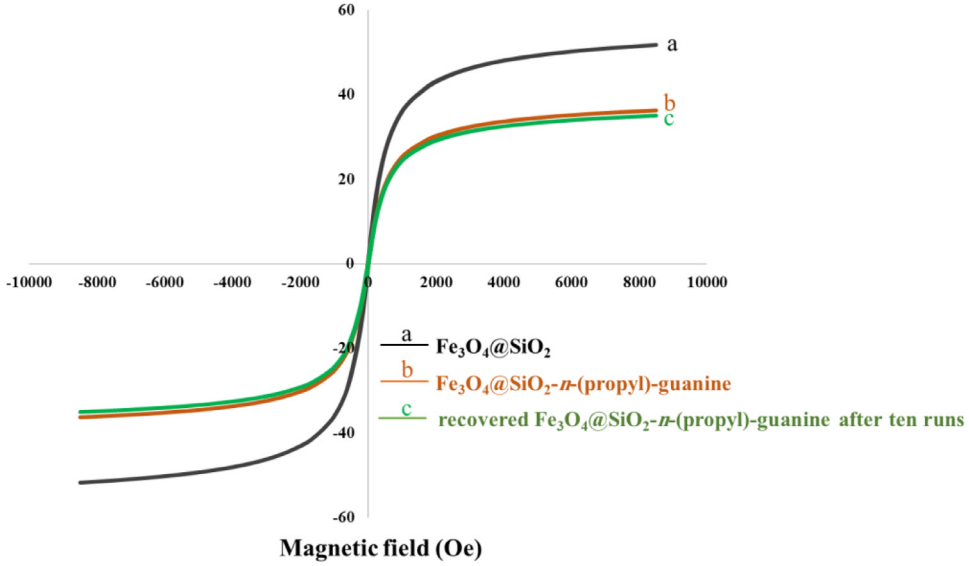

Fig. 6. Magnetization curve of the Fe_3O_4@SiO_2, Fe_3O_4@SiO_2-n-(propyl)-guanine and the recovered Fe_3O_4@SiO_2-n-(propyl)-guanine after ten runs

Fe_3O_4@SiO_2-n-(propyl)-guanine is presented in Fig. 1. For the IR spectrum of Fe_3O_4 nanoparticles (Fig. 1a), the absorption band appeared at 562 cm^{-1} which can be attributed to the stretching vibration of Fe–O bonds. In the spectrum in Fig. 1b, corresponding to the magnetite nanoparticles coated with silica, the signals at 562 and 1090 cm^{-1} are assigned to the stretching vibration of Fe–O and Si–O–Si bonds, respectively. In addition, the peak related to the silanol groups has appeared around 3100-3500 cm^{-1}. The FT–IR spectrum of Fe_3O_4@SiO_2–n-(propyl)-Cl is shown in Fig. 1c. In addition to the signals appearing in Fig. 1a and 1b, the peak related to the aliphatic C–H bond is visible around 2900-2950 cm^{-1}. In the IR spectra for Fe_3O_4@SiO_2-n-(propyl)-guanine (Fig. 1d), the peak around 3117 and 3320 cm^{-1} can be ascribed to the N–H band stretching frequency.

Quantitative determination of the organic groups stabilized on the surface of magnetite nanoparticles was studied by thermogravimetric analysis (Fig. 2). The weight loss of the catalyst between 30-800 °C as a function of temperature was determined using TGA (total weight loss is about 26.3 %). A slight weight loss below 250 °C corresponds to the removal of physically adsorbed water and involved approximately weight loss 3.8 %. 21% weight loss is observed in the temperature range of 250 to 550, which is related to the organic groups loaded on the surface of nanoparticles. This weight loss is equivalent to loading approximately 1 mmol of the organic group per gram catalyst.

Fig. 3 shows the XRD patterns of the Fe_3O_4@SiO_2–Cl, Fe_3O_4@SiO_2-n-(propyl)-guanine and the recovered Fe_3O_4@SiO_2-n-(propyl)-guanine after ten consecutive runs to check the phase purity. As can be seen in this Figure, the peaks at 2θ equal 30.1°, 35.4°, 43.1°, 53.4°, 57.1° and 62.6°, which can be indexed as (220), (311), (400), (511) and (440) lattice planes of cubic magnetite, respectively (JCPDS 19-629). The absence of peaks in $2\theta = 21.2$ (110) and $2\theta = 33.1$ (104) indicates that both goethite (α-FeOOH) and hematite (α-Fe_2O_3) are not present as impurities in the sample.

The morphology of the catalyst was investigated by SEM and HRTEM images (Fig. 4). Both images showed that the nanoparticles were present as uniform particles and the size of them was less than 15 nm. The obtained histogram (Fig. 4d) confirmed the fact that the size of distribution for 61 observed nanoparticles was a narrow normal one with an 8 nm average value. The HR-TEM image clearly shows that the catalyst support is core-shell and a layer of silica gel with approximately 2 nm thick covers the magnetic nanoparticles. The SEM image shown in Fig. 4c is of a recovered catalyst after ten consecutive runs. From the appearance of the image, it is clear that the size and morphology of the nanoparticles have been preserved.

The iron, silicon, oxygen, nitrogen and carbon atoms in the catalyst structure are well seen in the energy-dispersive X-ray analysis (EDX) (Fig. 5). Based on the data obtained from the EDX analysis and taking into account the nitrogen atom, the amount of organic group charged on the surface of magnetite nanoparticles is 0.99 mmol per gram catalyst, which is in good agreement with the result obtained from the TGA analysis.

Magnetic hysteresis measurement for the Fe_3O_4@SiO_2-n-(propyl)-guanine was done in an applied magnetic field at r.t., with the field sweeping from −8000 to 8000 Oersted. As shown in Fig. 6, the M (H) hysteresis loop for the sample was completely reversible, showing that the nanoparticles exhibited superparamagnetic characteristics. The hysteresis loops reached saturation up to the maximum applied magnetic field. The magnetic saturation value of the Fe_3O_4@SiO_2 was 48 emu g^{-1} at r.t. which was reduced to 32 emu g^{-1} after being coated with organic groups. In addition, there was no noticeable change in the magnetic saturation of the recovered catalyst after ten consecutive runs (Fig. 6c).

NMR-detected hydrogen/deuterium (H/D) exchange technique was used to determine the binding site of guanine to the propyltrimethoxy silane group. As shown in Fig. 7, the hydrogen attached to the nitrogen atom in a six-membered as well as the ones attached to the amino group have been removed in the H/D exchange spectrum and the binding site is the nitrogen atom in 5-membered ring.

After characterization of the Fe_3O_4@SiO_2-n-(propyl)-guanine, its catalytic activity was investigated for synthesis of some spirooxindole compounds in water (Scheme 2).

Initially, the multi-component reaction of dimedone (**1a**), malononitrile (**2a**), and isatin (**3a**) was selected as a model reaction to optimize the reaction time and efficiency by changing parameters such as solvent, catalyst, and reaction temperature (Table 1). The low efficiency of the product in the absence of catalyst and in water as solvent at 70°C showed that the presence of a catalyst was necessary to perform this reaction (Table 1, entry 1). The model reaction was then examined in the presence of different amounts of catalyst, and by using 0.02 g of it, the product **4a** was obtained with an excellent efficiency of 99% after 20 minutes of

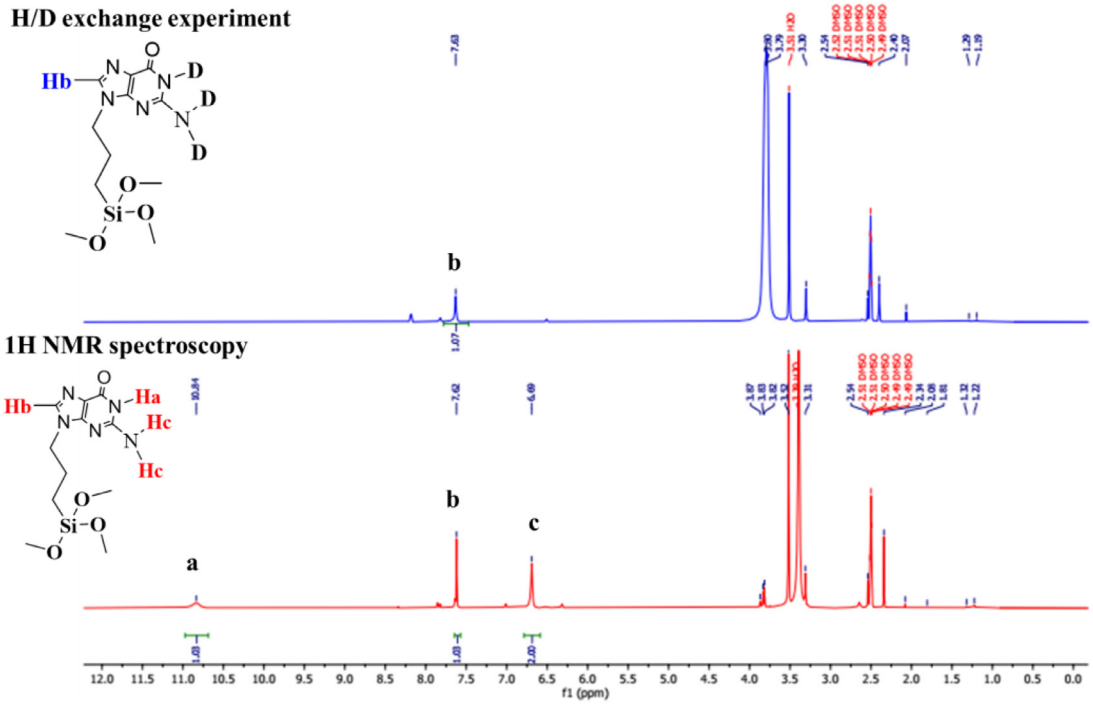

Fig. 7. H/D exchange method to determine the binding site of guanine to the trimethoxy silane propionate group.

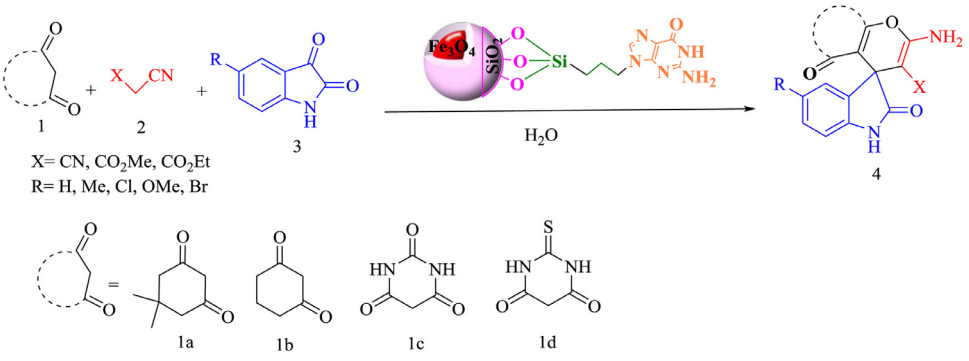

Scheme 2. Synthesis of some spirooxindole compounds in the presence of Fe_3O_4@SiO_2-n-(propyl)-guanine

Table 1
Optimization of the reaction conditions for the synthesis of spirooxindole **4a**.[a]

Yield (%)[b]	Temp. (°C)	Time (min)	Catalyst (mol%)	Solvent	Entry
Trace	70	300	-	H_2O	1
75	70	20	0.5	H_2O	2
88	70	20	1	H_2O	3
94	70	20	1.5	H_2O	4
99	70	20	2	H_2O	5
99	70	20	2	H_2O	[c]6
84	50	20	2	H_2O	7
67	r.t.	20	2	H_2O	8
96	70	20	2	EtOH/H_2O (1:1)	9
92	70	20	2	EtOH	10
89	70	20	2	DMSO	11
82	70	20	2	Toluene	12
88	70	20	2	PEG-400	13
79	reflux	60	2	DCM	14
84	reflux	60	2	MeOH	15

[a]Reaction conditions: dimedone (**1a**) (1 mmol), malononitrile (**2a**) (1 mmol), isatin (**3a**) (1 mmol), Fe_3O_4@SiO_2-n-(propyl)-guanine as the catalyst, solvent (5 mL). [b]Isolated yields. [c] Guanine as the catalyst.

Table 2
The structures of the synthesized spirooxindoles **4a-t**a. See Ref. [81].

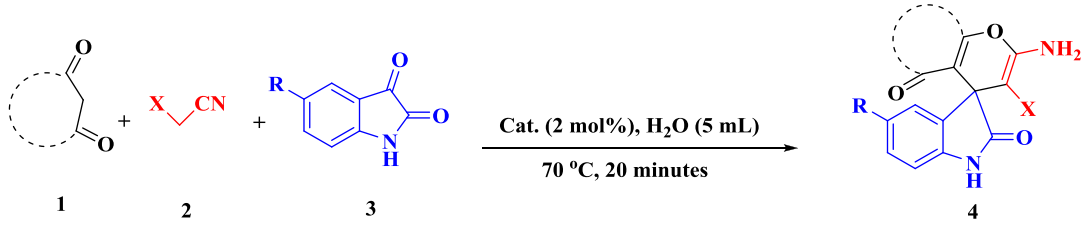

1 2 3 4

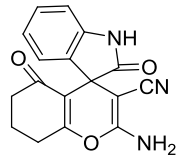

4a, 99%, m.p.305-308
(Lit. [75]; 307-310)

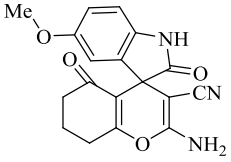

4b, 98%, m.p. 272-275
(Lit. [60]; 272-275)

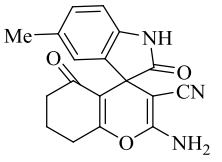

4c, 93%, m.p. 274-276
(Lit. [76]; 275–277)

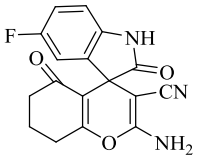

4d, 93%, m.p. 283-286
(Lit. [81]; 283–284)

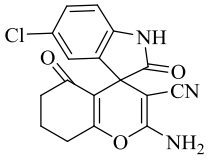

4e, 96%, m.p. 290-294
(Lit. [76]; 293-294)

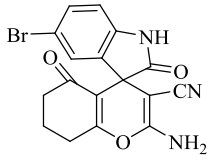

4f, 96%, m.p. 290-292
(Lit. [78]; 290-292)

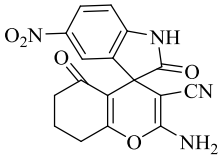

4g, 91%, m.p. 306-308
(Lit. [77]; 306-307)

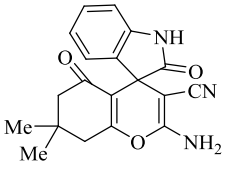

4h, 99%, m.p. 290-292
(Lit. [78]; 290-292)

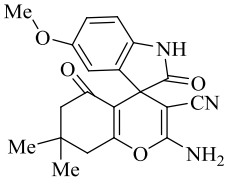

4i, 99%, m.p.270-272
(Lit. [60]; 270-272)

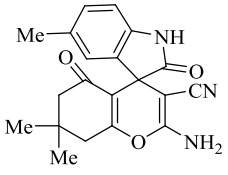

4j, 95%, m.p. 276-279
(Lit. [78]; 279-280)

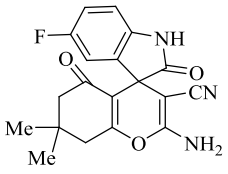

4k, 97%, m.p.273-275
(Lit. [81]; 293 (dec.)

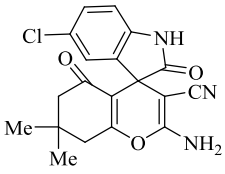

4l, 98%, m.p. 285-288
(Lit. [76]; 288289)

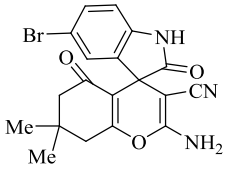

4m, 97%, m.p. 307-309
(Lit. [78]; <300)

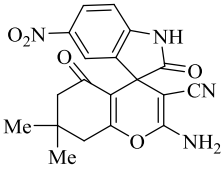

4n, 94%, m.p. 302-305
(Lit. [79]; 302-304)

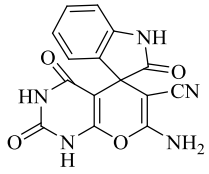

4o, 88%, m.p. 275-276
(Lit. [14]; 276-278)

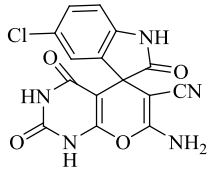

4p, 87%, m.p. 235-239
(Lit. [14]; 237-240)

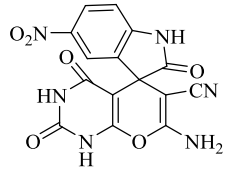

4q, 84%, m.p. 285-288
(Lit. [14]; 286-288)

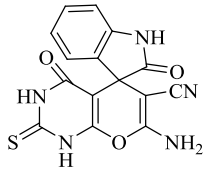

4r, 81%, m.p. 236-238.
(Lit. [14]; 235-237)

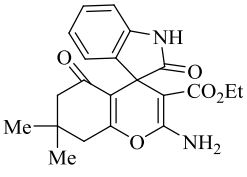

4s, 91%, m.p. 256-259
(Lit. [43]; 258-260)

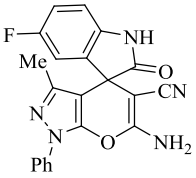

4t, 94%, m.p. 233-235
(Lit. [81]; 242 (dec.))

aReaction conditions: **1** (1 mmol), **2** (1 mmol) and **3** (1 mmol), catalyst (0.02 g), H2O (5mL), 70 °C. The yields refer to the isolated pure products.

Table 3
The structures of the synthesized bis-spirooxindole derivatives **6a-i**a

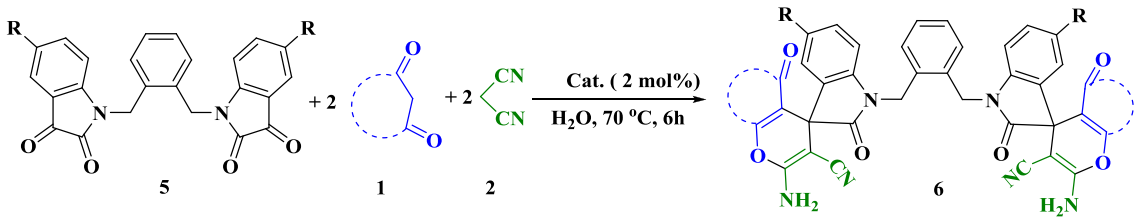

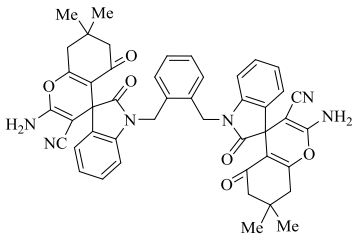

6a, 97%, m.p. 303-304

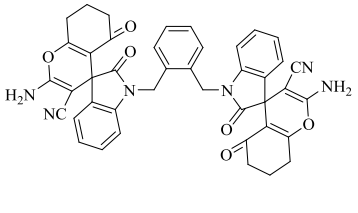

6b, 94%, m.p. 298-300

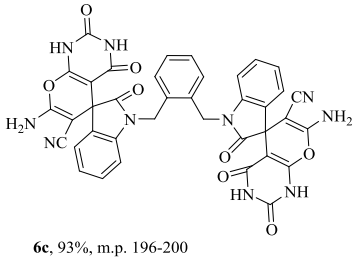

6c, 93%, m.p. 196-200

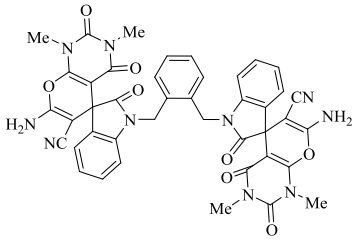

6d, 90%, m.p. 233-237

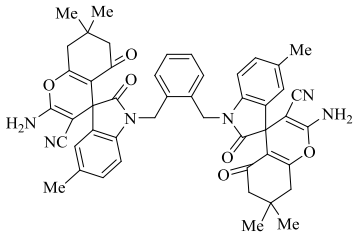

6e, 93%, m.p. 204-208

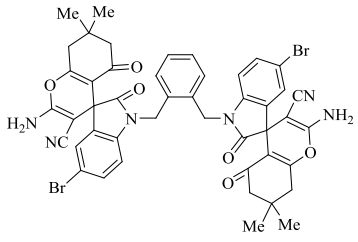

6f, 96%, m.p. 212-215

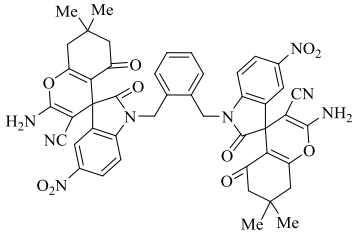

6g, 87%, m.p. 316-318;

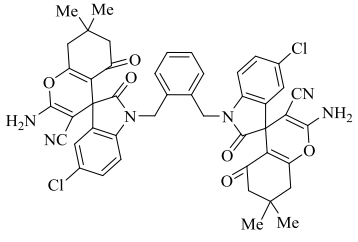

6h, 91%, m.p. 325-328

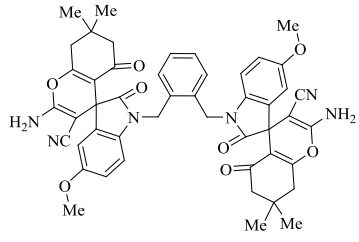

6i, 95%, m.p. >200

aReaction conditions: **1** (2 mmol), **2** (2 mmol) and **5** (1 mmol), catalyst (2 mol%), H2O (5 mL), 70 °C, 6 h. The yields refer to the isolated pure products.

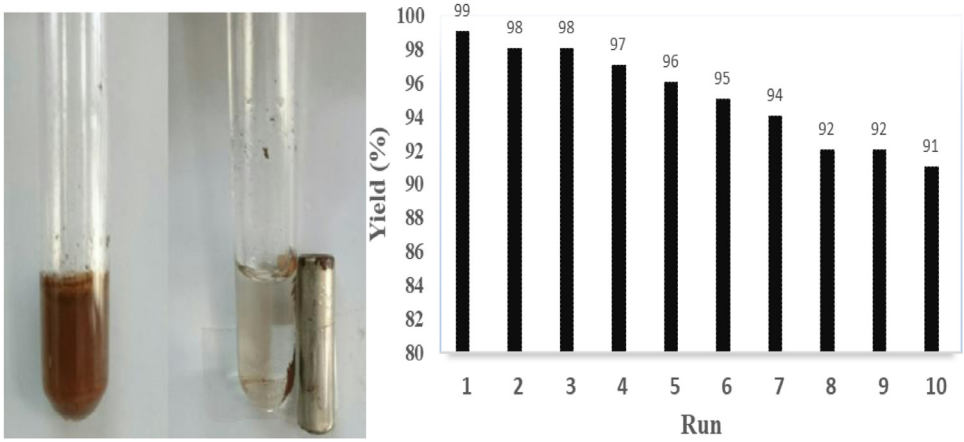

Fig. 8. Reusability results of the catalyst in the preparation of product **4a**

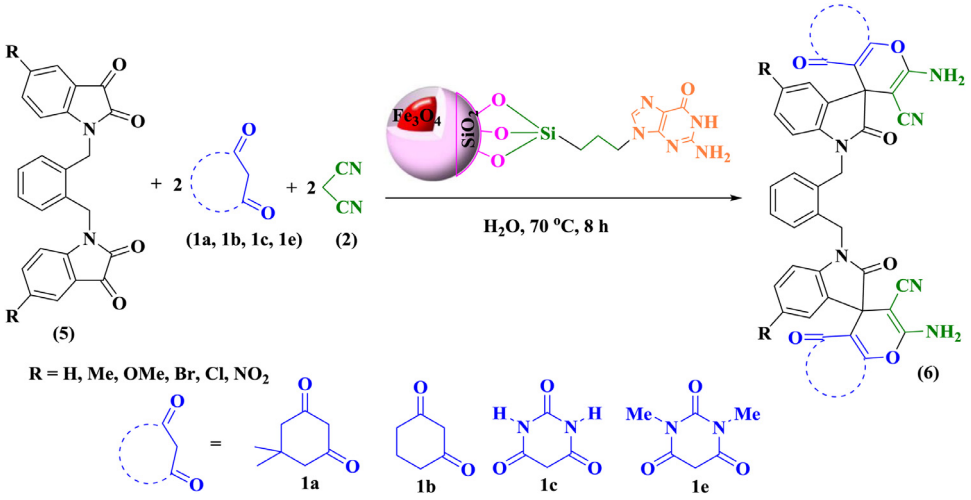

Scheme 3. Synthesis of bis-spirooxindole derivatives

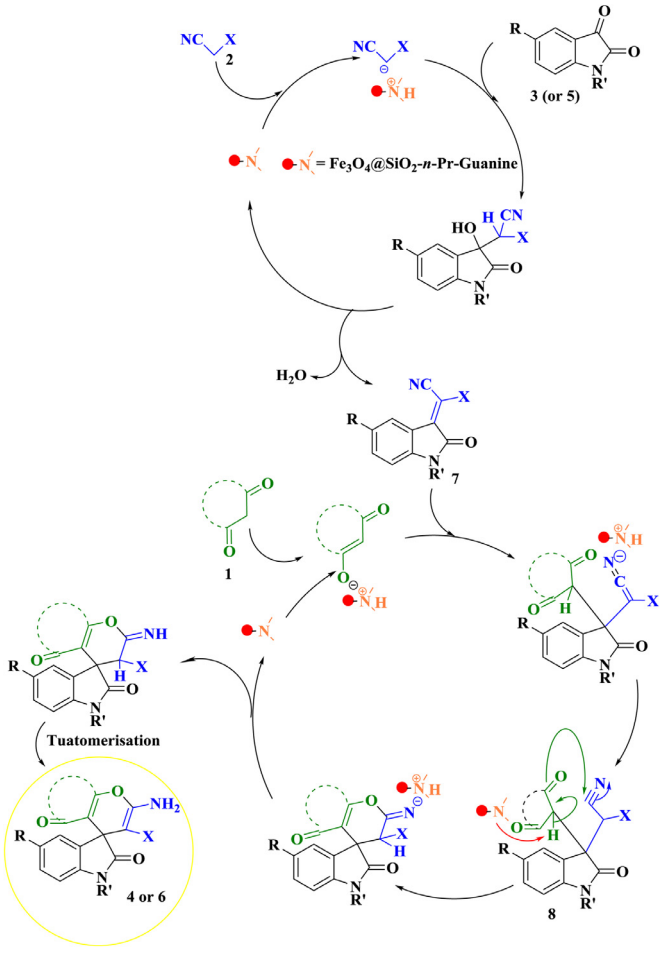

Scheme 4. A plausible reaction mechanism

the reaction time (Table 1, entries 2-5). The model reaction was also tested in the presence of guanine (0.02 g, 0.13 mmol) in water at 70°C and the corresponding product was obtained in excellent yield (99% yield), but the reaction in the presence of the Fe_3O_4@SiO_2-n-(propyl)-guanine was cleaner and the product easier to separate. At the same time, the catalyst was easily separated from the reaction mixture, by applying an external magnet and reused (Table 1, entry 6). As the temperature dropped, the efficiency of the product also decreased. These results showed that the temperature played an effective role in reaction efficiency (Table 1, entries 7-8). In another effort, the model reaction was carried out in various solvents such as EtOH/H_2O (1:1), EtOH, DMSO, toluene, PEG-400, CH_2Cl_2, and MeOH (Table 2, entries 9-15). In all cases, the efficiency was good, although there was the highest efficiency in water solvent.

With the optimized reaction conditions in hand, the scope and efficiency of this protocol was explored by employing different isatin derivatives, malononitrile and dicarbonyl compounds and the results were summarized in Table 2. As shown in this table, a series of differently substituted isatins with electron withdrawing and electron donating groups reacted with malononitrile and 1,3-cyclohexanedione or dimedone and the desired products were obtained in excellent yields (products **4a-n**). Also, the other carbonyl compounds such as barbituric acid (products **4o-q**) and thiobarbituric acid (product **4r**) were easily transformed into the corresponding products in good yields. The product of the reaction between dimedone, isatin, and ethyl cyanoacetate was also isolated by 91% efficiency. Moreover, when the 5-methyl-2-phenyl-2,4-dihydro-3H-pyrazol-3-one reacted with malononitrile and 5-fluoroisatin, the corresponding product **4t** was isolated with 94% yield. All isolated products were known and gave satisfactory physical and spectral data (melting points, FT-IR, and ^{1}H and ^{13}C NMR) compared with those reported in the literature.

The structures of the synthesized bis-spirooxindoles are shown in Table 3. Generally speaking, some 1,3-dicarbonyl compounds (namely dimedone, 1,3-cyclohexanedione, barbituric acid, and dimethyl barbituric acid) were treated with bis(isatin) and its derivatives and malononitrile to give the corresponding products in good yields (Table 3, products **6a-i**).

A plausible reaction mechanism for the synthesis of compounds **4** or **6** in the presence of Fe_3O_4@SiO_2–n-(propyl)-guanine is shown in Scheme 4. At first, the malonitrile derivatives **2** is converted to the corresponding carbanion nucleophile in the presence of the catalyst followed by the fast Knoevenagel condensation between isatine derivative **3** and carbanion compound **2** to produce the olefin **7**. Then, Michael addition of olefin **7** with 1,3-dicarbonyl compound **1** followed by proton transfer and tautomerization provides the corresponding mono or bis-spirooxindoles **4** or **6**.

Easy separation by external magnet and reusability up to ten times are prominent features of our catalytic system. Reusability of the catalyst was studied in the preparation of compound **4a**. After completion of the reaction in the first run, the catalyst was easily

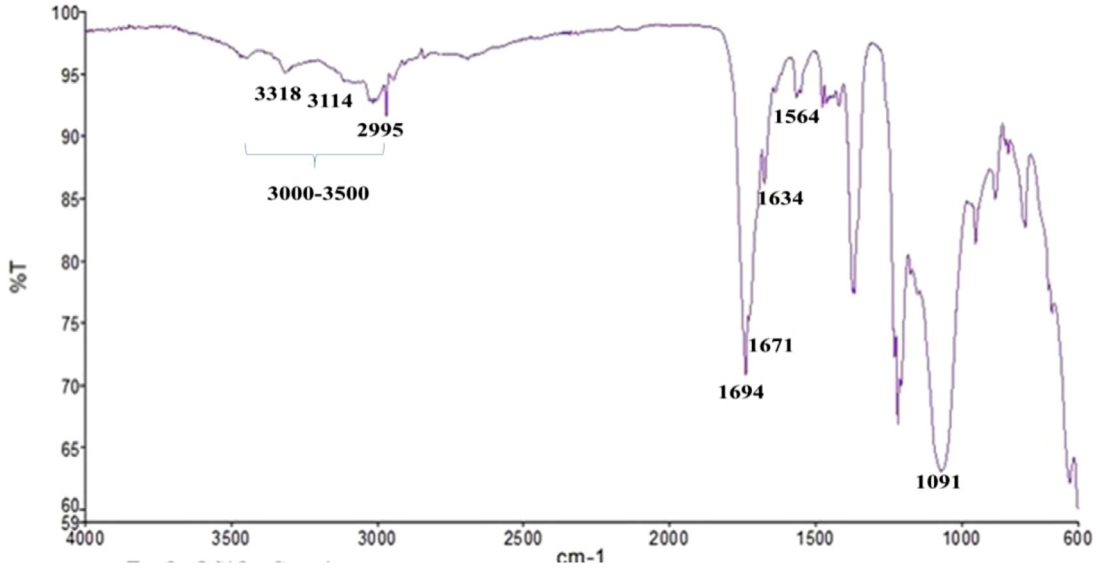

Fig. 9. FT-IR spectra of recovered Fe_3O_4@SiO_2-n-(propyl)-guanine after ten consecutive runs

separated from the reaction mixture by using an external magnet; it was washed with distilled water (2 × 5 mL), ethanol (2 × 5 mL), and acetone (2 × 5 mL) respectively, dried at ambient temperature and immediately used in the next step. The reaction was repeated for up to ten consecutive runs without significant change in the efficiency of the reaction (Fig. 8). As mentioned above, and based on the recorded analyzes of the recovered catalyst after ten consecutive runs, the size, morphology and magnetic properties of the catalyst did not change much.

Fig. 9 also shows the FT-IR spectrum of the recovered catalyst. As can be seen, it does not differ from the spectrum of the original catalyst, and all the functional groups in the structure of the catalyst are clearly visible.

In summary, the Fe_3O_4@SiO_2–n-(propyl)-guanine was used as an efficient and recyclable catalytic system for the one-pot synthesis of spirooxindole derivatives in aqueous media using readily available starting materials. This heterogeneous and magnetically separable catalyst was used for ten consecutive runs without any noticeable reduction in efficiency. The advantages of the presented methodology are its simplicity, short reaction times, recoverable catalyst, high yields, easy work-up, aqueous media and environmentally benign mild reaction conditions.

Declaration of Competing Interest

The authors declare that they have no known competing financial interests or personal relationships that could have appeared to influence the work reported in this paper.

Acknowledgment

We are thankful to Persian Gulf University Research Council for partial support of this work.

References

[1] G.J. Kelly, F. King, M. Kett, Green. Chem. 4 (2002) 392–399.
[2] R.A. Sheldon, H. van Bekkum, in: Fine chemicals through heterogeneous catalysis: Solid base catalysts, chap 7. Wiley-VCH, Weinheim, 2001, pp. 309–350.
[3] R.K. Zeidan, S.-J. Hwang, M.E. Davis, Angew. Chem. Int. Ed 45 (2006) 6332–6335.
[4] S. Shylesh, A. Wagner, A. Seifert, S. Ernst, W.R. Thiel, Chem. Eur. J 15 (2009) 7052–7062.
[5] P.H. Toy, Y. Lam, Solid-phase organic synthesis: concepts, strategies, and applications, eds, Wiley, Weinheim, 2012.
[6] S. Rostamnia, E. Doustkhah, RSC Adv. 4 (2014) 28238–28248.
[7] J. Weitkamp, M. Hunger, U. Rymsa, Micropor. Mesopor. Mater 48 (2001) 255–270.
[8] T. Yokoi, Y. Kubota, T. Tatsumi, Appl. Catal. A Gen. (2012) 14–37 **421-422**.
[9] M. Bartók, Chem. Rev 110 (2010) 1663–1705.
[10] K. Ding, Y. Uozumi, Handbook of asymmetric heterogeneous catalysis, eds, Wiley-VCH, Weinheim, 2008.
[11] K. Niknam, A. Jamali, Chin. J. Catal. 33 (2012) 1840–1849.
[12] K. Niknam, N. Borazjani, R. Rashidian, A. Jamali, Chin. J. Catal. 34 (2013) 2245–2254.
[13] K. Niknam, M. Sadeghi Habibabad, A. Deris, N. Aeinjamshid, Monatsh. Chem. 144 (2013) 987–992.
[14] K. Niknam, P. Abolpour, Monatsh. Chem. 146 (2015) 683–690.
[15] T. Tamoradi, A. Ghorbani-Choghamarani, M. Ghadermazi, New J. Chem. 41 (2017) 11714–11721.
[16] M. Afradi, N. Foroughifar, H. Pasdar, H. Moghanian, N. Foroughifar, Appl. Organometal. Chem. 31 (2017) e3683.
[17] T. Tamoradi, M. Ghadermazi, A. Ghorbani-Choghamarani, Appl. Organometal. Chem 32 (2017) e3974.
[18] Z. Zhang, Y. Xiao, Y. Lei, J. Tang, X. Qiao, Sci. Total Environ 738 (2020) 139742.
[19] M. Ghaedi, K. Niknam, S. Zamani, H.A. Larki, M. Roosta, M. Soylak, Mat. Sci. Eng. C-Mater. 33 (2013) 3180–3189.
[20] B. Biswas, A. Kumar, A.C. Fernandes, K. Saini, S. Negi, U.D. Muraleedharan, T. Bhaskar, Bioresource Technol. 307 (2020) 123232.
[21] V. Ahluwalia, R. Varma, Green solvents for organic synthesis, Alpha Science International, Oxford, 2009.
[22] P.J. Dunn, Chem. Soc. Rev. 41 (2012) 1452–1461.
[23] R.N. Butler, A.G. Coyne, Chem. Rev. 110 (2010) 6302–6337.
[24] M.B. Gawande, V.D.B. Bonifaćio, R. Luque, P.S. Brancoa, R.S. Varma, Chem. Soc. Rev. 42 (2013) 5522–5551.
[25] Y.–C. Wang, J.L. Wang, K.S. Burgess, J.–W. Zhang, Q.–M. Zheng, Y.–D. Pu, L.–J. Yan, X.–B. Chen, RSC Adv 8 (2018) 5702–5713.
[26] C.-B. Cui, H. Kakeya, H. Osada, Tetrahedron 52 (1996) 12651–12666.
[27] G. Palmisano, R. Annunziata, G. Papeo, M. Sisti, Tetrahedron: Asymmetry 7 (1996) 1–4.
[28] J.F. Da Silva, S.J. Garden, A.C. Pinto, J. Braz. Chem. Soc. 12 (2001) 273–324.
[29] W.-H. Wong, P.-B. Lim, C.-H. Chuah, Phytochemistry 41 (1996) 313–315.
[30] M. Kates, L. Marion, Can. J. Chem. 29 (1951) 37–45.
[31] B. Yu, D.-Q. Yu, H.-M. Liu, Eur. J. Med. Chem. 97 (2015) 673–698.
[32] J.-S. Wu, X. Zhang, Y.-L. Zhang, J.-W. Xie, Org. Biomol. Chem. 13 (2015) 4967–4975.
[33] S. Tiwari, P. Pathak, R. Sagar, Bioorg. Med. Chem. Lett. 26 (2016) 2513–2516.
[34] S. Haddad, S. Boudriga, T.N. Akhaja, J.P. Raval, F. Porzio, A. Soldera, M. Askri, M. Knorr, Y. Rousselin, M.M. Kubicki, New J. Chem. 39 (2015) 520–528.
[35] F. Rouatbi, M. Askri, F. Nana, G. Kirsch, D. Sriram, P. Yogeeswari, Tetrahedron Lett 57 (2016) 163–167.
[36] G. Kumari, M. Modi, S.K. Gupta, R.K. Singh, Eur. J. Med. Chem. 46 (2011) 1181–1188.
[37] M. Dabiri, M. Bahramnejad, M. Baghbanzadeh, Tetrahedron 65 (2009) 9443–9447.
[38] Y. Li, H. Chen, C. Shi, D. Shi, S. Ji, J. Comb. Chem. 12 (2010) 231–237.
[39] K. Jadidi, R. Ghahremanzadeh, A. Bazgir, J. Comb. Chem. 11 (2009) 341–344.
[40] G.M. Ziarani, A. Badiei, S. Mousavi, N. Lashgari, A. Shahbazi, Chin. J. Catal. 33 (2012) 1832–1839.
[41] B. Sadeghi, Z. Lasemi, R. Azimi, Orient. J. Chem. 31 (2015) 1175–1179.

[42] Y.M. Litvinov, V.Y. Mortikov, A.M. Shestopalov, J. Comb. Chem. 10 (2008) 741–745.
[43] P. Saluja, K. Aggarwal, J.M. Khurana, Synth. Commun. 43 (2013) 3239–3246.
[44] B. Karmakar, A. Nayak, J. Banerji, Tetrahedron Lett 53 (2012) 5004–5007.
[45] R.-Y. Guo, P. Wang, G.-D. Wang, L.-P. Mo, Z.-H. Zhang, Tetrahedron 69 (2013) 2056–2061.
[46] S. Gao, C.H. Tsai, C. Tseng, C.-F. Yao, Tetrahedron 64 (2008) 9143–9149.
[47] Z.-Q. Liu, Z.-W. Xiang, Q. Wu, X.-F. Lin, Biochimie 95 (2013) 1462–1465.
[48] H.R. Safaei, M. Shekouhy, A. Shirinfeshan, S. Rahmanpur, Mol. Divers. 16 (2012) 669–683.
[49] A. Dandia, A.K. Jain, D.S. Bhati, Synth. Commun. 41 (2011) 2905–2919.
[50] S.-L. Zhu, S.-J. Ji, Y. Zhang, Tetrahedron 63 (2007) 9365–9372.
[51] N. Lashgari, G.M. Ziarani, A. Badiei, M. Zarezadeh-Mehrizi, J. Heterocycl. Chem. 51 (2014) 1628–1633.
[52] S.P. Satasia, P.N. Kalaria, J.R. Avalani, D.K. Raval, Tetrahedron 70 (2014) 5763–5767.
[53] R. Ghahremanzadeh, Z. Rashid, A.H. Zarnani, H. Naeimi, Appl. Catal. A Gen. 467 (2013) 270–278.
[54] Y. Zou, Y. Hu, H. Liu, D. Shi, ACS Comb. Sci. 14 (2011) 38–43.
[55] A. Thakur, M. Tripathi, U.C. Rajesh, D.S. Rawat, RSC Adv 3 (2013) 18142–18148.
[56] M. Mamaghani, K. Tabatabaeian, M. Pourshiva, R.H. Nia, J. Chem. Res. 39 (2015) 314–317.
[57] K. Niknam, A. Piran, Z. Karimi, J. Iran, Chem. Soc. 13 (2016) 859–871.
[58] A. Allahresani, B. Taheri, M.A. Naseri, Res. Chem. Intermed. 44 (2018) 1173–1188.
[59] S. Agarwal, M. Kidwai, M. Nath, Chem. Select 4 (2019) 2135–2139.
[60] M. Bashkar, M. Bavadi, E. Ghaderi, K. Niknam, Mol. Divers. (2020) 24 Print ahead.
[61] W.-B. Chen, Z.-J. Wu, Q.-L. Pei, L.-F. Cun, X.-M. Zhang, W.-C. Yuan, Org. Lett. 12 (2010) 3132–3135.
[62] M. Kidwai, A. Jain, S. Bhardwaj, Mol. Divers. 16 (2012) 121–128.
[63] M.A. Nasseri, S.M. Sadeghzadeh, J. Iran. Chem. Soc. 10 (2013) 1047–1056.
[64] M. Esmaeilpour, J. Javidi, M. Divar, J. Magn. Magn. Mater. 423 (2017) 232–240.
[65] N. Mohammadian, B. Akhlaghinia, Res. Chem. Intermed. 45 (2019) 4737–4756.
[66] K. Niknam, A. Gharavi, M.R. Hormozi Nezhad, F. Panahi, M.T. Sharbati, Synthesis (2011) 1609–1615.
[67] K. Niknam, M. Sadeghi Habibabad, A. Deris, F. Panahi, M.R. Hormozi Nezhad, J. Iran. Chem. Soc. 10 (2013) 527–534.
[68] K. Niknam, A. Deris, F. Panahi, M.R. Hormozi Nezhad, J. Iran. Chem. Soc. 10 (2013) 1291–1296.
[69] K. Niknam, A. Deris, F. Panahi, Chin. J. Catal. 34 (2013) 718–722.
[70] M. Makvandi, F. Abiar Dil, A. Malekzadeh, M. Baghernejad, K. Niknam, Iran. J. Catal. 3 (2013) 221–228.
[71] K. Niknam, R. Rashidian, A. Jamali, Scientia Iranica C 20 (2013) 1863–1870.
[72] K. Niknam, N. Borazjani, Monatsh. Chem. 147 (2016) 1129–1135.
[73] K. Niknam, A.R. Hosseini, Org. Chem. Res. 3 (2017) 16–24.
[74] K. Niknam, H. Hashemi, M. Karimzadeh, D. Saberi, J. Iran, Chem. Soc. 17 (2020) 3095–3178.
[75] K. Hemmat, M.A. Nasseri, A. Allahresani, S. Ghiami, J. Organomet. Chem. 903 (2019) 120996.
[76] B. Sadeghi, Z. Lasemi, R. Azimi, Orient. J. Chem. 31 (2015) 1175–1179.
[77] M. Mamaghani, K. Tabatabaeian, M. Pourshiva, R.H. Nia, J. Chem. Res. 39 (2015) 314–317.
[78] Y. Li, H. Chen, C. Shi, D. Shi, S. Ji, J. comb. Chem. 12 (2010) 231–237.
[79] G.M. Ziarani, A. Badiei, S. Mousavi, N. Lashgari, A. Shahbazi, Chin. J. Catal. 33 (2012) 1832–1839.
[80] M. Shekouhy, A. Khalafi-Nezhad, Green Chem. 17 (2015) 4815–4829.
[81] A. Hasaninejad, N. Golzar, M. Beyrati, A. Zare, M.M. Doroodmand, J. Mol. Catal. A: Chem. 372 (2013) 137–150.